Device-quality, reconfigurable metamaterials from shape-directed nanocrystal assembly

Wenjie Zhou[a,b,1], Zizhuo Liu[a,c,1], Ziyin Huang[a,d], Haixin Lin[a,b], Devleena Samanta[a,b], Qing-Yuan Lin[a,d], Koray Aydin[a,c,2], and Chad A. Mirkin[a,b,d,2]

[a]International Institute for Nanotechnology, Northwestern University, Evanston, IL 60208; [b]Department of Chemistry, Northwestern University, Evanston, IL 60208; [c]Department of Electrical and Computer Engineering, Northwestern University, Evanston, IL 60208; and [d]Department of Materials Science and Engineering, Northwestern University, Evanston, IL 60208

Contributed by Chad A. Mirkin, June 30, 2020 (sent for review April 10, 2020; reviewed by Rafal Klajn and Nicholas A. Kotov)

Anchoring nanoscale building blocks, regardless of their shape, into specific arrangements on surfaces presents a significant challenge for the fabrication of next-generation chip-based nanophotonic devices. Current methods to prepare nanocrystal arrays lack the precision, generalizability, and postsynthetic robustness required for the fabrication of device-quality, nanocrystal-based metamaterials [Q. Y. Lin et al. Nano Lett. 15, 4699–4703 (2015); V. Flauraud et al., Nat. Nanotechnol. 12, 73–80 (2017)]. To address this challenge, we have developed a synthetic strategy to precisely arrange any anisotropic colloidal nanoparticle onto a substrate using a shallow-template-assisted, DNA-mediated assembly approach. We show that anisotropic nanoparticles of virtually any shape can be anchored onto surfaces in any desired arrangement, with precise positional and orientational control. Importantly, the technique allows nanoparticles to be patterned over a large surface area, with interparticle distances as small as 4 nm, providing the opportunity to exploit light–matter interactions in an unprecedented manner. As a proof-of-concept, we have synthesized a nanocrystal-based, dynamically tunable metasurface (an anomalous reflector), demonstrating the potential of this nanoparticle-based metamaterial synthesis platform.

gold nanocrystals | DNA-mediated assembly | surface patterning | reconfigurable metamaterials

Optical metamaterials are artificial materials engineered to have optical properties that exceed what is offered by nature (1). These materials often contain nanoscale features with dimensions comparable to or less than the wavelength of light, giving rise to light–matter interactions that are completely different from those of flat surfaces (2–9). Conventionally, such features are fabricated via top-down methods such as templated thin-film deposition or etching that results in planar architectures (4, 5, 10). Optical devices made from these metamaterials suffer from polycrystallinity and surface roughness, inherent to the techniques used to fabricate them (10). Recent advances in the synthesis of inorganic colloidal nanoparticles (NPs) with desired sizes, shapes, compositions, and crystallinities (11), provide access to a new set of high-quality materials that can serve as building blocks for generating metamaterials through a bottom-up approach (12–17). The ability to precisely control the arrangement of colloidal nanocrystals of any arbitrary shape onto surfaces would provide an avenue for exploring a broad range of metamaterials that are otherwise synthetically unattainable and creating a combinatorial search platform for screening emergent properties (4, 5, 17).

Over the past decade, colloidal crystal engineering with DNA has emerged as a powerful strategy to assemble NP-based materials into hierarchical structures with different lattice symmetries and crystal habits (18–25). Recently, DNA-mediated assembly has been combined with top-down lithography to generate dynamically responsive, surface-bound colloidal NP superlattices (1, 14, 15, 26, 27). In this strategy, DNA-modified NPs are assembled in a layer-by-layer fashion into lithographically defined pores. Unlike traditional top-down fabrication approaches with which nonprismatic structures are challenging to fabricate, template-confined, DNA-mediated assembly enables control over the placement of NPs of different shapes, sizes, and compositions in the out-of-plane direction (15). Moreover, combining the tunability of DNA length with device design yields a highly tailorable system with actively tunable properties that is not possible with conventional techniques. However, in-plane structural control such as the position and orientation of the anchored NPs, which is critical for achieving device-quality metamaterials, has been unobtainable due to the relatively large pore dimensions (width and depth) necessary for out-of-plane assembly. Specifically, it was determined that in order to maintain a satisfactory yield (>95%) of the multilayered structures, the width of the pores must be ~1.4 times the hydrodynamic diameter, d, of the NPs (i.e., the diameter of the NP + twice the thickness of the DNA shell) (26). This constraint results in two major disadvantages. First, lateral and angular precisions are sacrificed as the first layer of NPs anchor in random orientations at random positions within the large pores. Second, the interparticle distance (center-to-center) is restricted by the NP size and can only be as small as 1.4d. For example, two cubes with 80-nm edge lengths could be placed with an average gap of ~110 nm between them (*SI Appendix*, Fig. S2), a limitation that poses a major impediment to the design of optically active metamaterials. Here, we report via a shallow-template strategy that DNA-modified colloidal nanocrystals

Significance

Colloidal nanocrystals with defined sizes and shapes are ideal building blocks for nanofabrication. However, the ability to arbitrarily arrange them on surfaces with control over their orientation remains elusive. Here we report a shallow-template-assisted DNA-mediated assembly strategy to precisely arrange colloidal nanocrystals on surfaces, with single-particle control across submillimeter areas. In addition, the oligonucleotide bonds between the nanocrystals and substrate can be reversibly expanded and contracted enabling postsynthetic tunability of the assembled structures. Using this approach, we synthesized a nanocrystal-based, dynamically tunable metasurface (an anomalous reflector), thereby illustrating the potential for unique device construction via DNA programmable assembly.

Author contributions: W.Z. and Q.-Y.L. designed research; W.Z., Z.L., Z.H., and H.L. performed research; W.Z., Z.L., Z.H., H.L., Q.-Y.L., and C.A.M. analyzed data; and W.Z., Z.L., D.S., K.A., and C.A.M. wrote the paper.

Reviewers: R.K., Weizmann Institute of Science; and N.A.K., University of Michigan–Ann Arbor.

The authors declare no competing interest.

[1]W.Z. and Z.L. contributed equally to this work.

[2]To whom correspondence may be addressed. Email: aydin@northwestern.edu or chadnano@northwestern.edu.

This article contains supporting information online at https://www.pnas.org/lookup/suppl/doi:10.1073/pnas.2006797117/-/DCSupplemental.

First published August 17, 2020.

of almost any shape can be precisely arranged onto a substrate, with control over position, symmetry, and orientation as well as the facet of the NP interacting with the surface. Importantly, this technique can be used to place NPs less than 100 nm away from one another, enabling one to deliberately adjust the optical coupling between the particles. Using this approach, we have fabricated a dynamically tunable anomalous reflector.

Results and Discussion

To obtain multilayered structures, large pores (both in width and depth) are required to accommodate the particles that define the line stacks and facilitate their diffusion and subsequent adsorption onto the lithographically defined DNA bonding sites. The dimensions of these pores limit how close two nanostructures can be placed in-plane and therefore the types of optically active metamaterials that can be produced and studied. In contrast, two-dimensional (2D) metamaterials formed from single layers of anisotropic particles, should not require such large pores, and therefore, we hypothesized that low-aspect-ratio shallow pores, which reduce the barrier to diffusion without affecting the strength of adsorption, would result in improved accuracy with respect to lateral and angular particle placement. To achieve

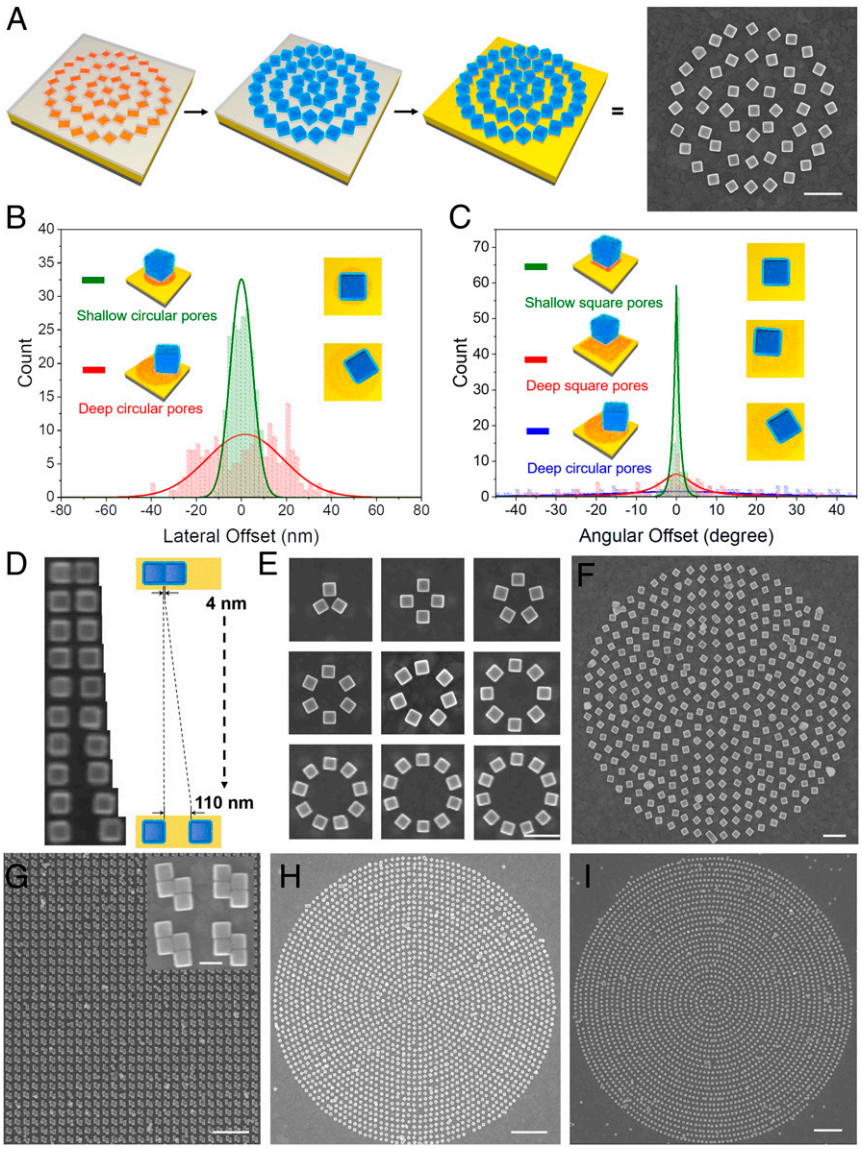

Fig. 1. Positional and orientational control over anchoring of prismatic NPs using shallow pores. (*A*) Schematic illustration of precise 2D arrangement of DNA-functionalized nanocubes. Using EBL, pores are patterned into a PMMA layer coated onto a gold-coated silicon substrate. The bases of lithographically defined pores (square gold sites) are functionalized with thiolated DNA (red); nanocubes functionalized with complementary DNA (blue) are allowed to assemble into the pores. The sacrificial PMMA template is dissolved after the assembly is complete. (*B*) Statistical analysis of lateral offset: comparison between 50-nm-deep circular pores (green) and 200-nm-deep circular pores (red). A minimal pore size for each pore depth was chosen, where an adsorption yield of >95% could be achieved. Shallow pores: diameter = 130 nm, *Top* schemes; deep pores: diameter = 190 nm, *Bottom* schemes). One hundred sites were counted for each pore depth. (*C*) Statistical analysis of angular offset: comparison among 50-nm-deep square pores, 200-nm-deep square pores, and 200-nm-deep circular pores. A minimal pore size for each design was chosen, where an adsorption yield of >95% can be achieved. Shallow square pores: edge length = 95 nm, *Top* schemes; deep square pores: edge length = 170 nm, *Middle* schemes; deep circular pores: diameter = 190 nm, *Bottom* schemes. (*D*) A cube dimer (edge length = 80 nm) arranged with gradually increasing distance, from 4 nm to 110 nm. (*E–I*) SEM images of nanocubes arranged in arbitrary patterns. Nanocubes with edge lengths of 80 nm were used for all experiments. (Scale bars: 300 nm (*A*, *E*, and *F*); 1 μm (*G*, *H*, and *I*); 100 nm (*G*, *Inset*).)

"adsorption-dominated" confinement, we used electron-beam lithography (EBL) to pattern a uniform array of shallow pores into a thin (~50 nm) layer of poly(methyl methacrylate) (PMMA) spin-coated onto a gold-coated silicon substrate (see *SI Appendix*, Table S2 for spin-coating parameters) (28). The exposed gold sites were subsequently functionalized with propylthiolated DNA (sequence provided in *SI Appendix*, Table S1). NPs functionalized with complementary DNA, with a height (i.e., hydrodynamic diameter, d) larger than the pore depth, were assembled into the pores, creating partially embedded NP architectures. Upon dissolution of the PMMA template, the assembled NPs maintain their anchoring positions (Fig. 1*A*). The dimensions of the patterned pores directly impact the yield of the assembled structures—NPs cannot assemble into pores that are too small (pore dimensions compared to d), and lateral precision is lost when the pores are too large due to capillary forces between the broad faces of the NPs and the walls of the pores (Fig. 1*B* and *SI Appendix*, Fig. S5). We studied the assembly of nanocubes into pores with different shapes and dimensions. We chose nanocubes because they are readily synthesized (29), have only one type of facet (square), and are, therefore, excellent candidates for evaluating orientation control. Our results indicate that by reducing pore depth, smaller cross-sectional pore dimensions can be realized, leading to smaller lateral offsets with regard to particle placement but comparably high adsorption yields (>95%) (Fig. 1 *B* and *C*). Importantly, when the pore dimensions are comparable to d, the orientation of the NP can also be controlled by carefully designing the pore depth and shape.

With this shallow-pore strategy, it should be possible to control the orientation of nanocubes, by designing pores that mirror their square-shaped facets. Indeed, when 95-nm edge length square pores with 50-nm pore depths were used, cubes with 80-nm edge lengths can be assembled into 2D superstructures with tight control over cube orientation (Fig. 1). For comparative purposes, although nanocube orientation can be partially controlled with deeper pores with larger cross-sections (*SI Appendix*, Fig. S2), significant lateral offsets are observed, and it is not possible to place two nanocubes closer than ~0.8d from each other (the gap between the NPs). The use of shallow pores with smaller cross-sectional dimensions eliminates these problems, allowing NPs to be placed as close as 4 nm from each other, a distance more than an order of magnitude closer than the size of the NPs (Fig. 1*D*). Geometrically speaking, cubes are relatively simple structures. However, we set out to develop a universal strategy to control the oriented attachment of NPs of almost any given shape. We arrived at this strategy by exploring how the shallow-pore template strategy and pore-shape control could be combined to direct the orientations of four representative nonprismatic NPs, namely, octahedra, cuboctahedra, small triambic icosahedra, and decahedra (Fig. 2 *A–D*). Remarkably, in all four cases adsorption yields >90% were achieved. In general, for a given NP of any shape and size, the pore depth and shape can be modulated to control its orientation. However, for a nonprismatic NP, the required pore depth and shape are interrelated in that changing the thickness of the PMMA template changes the pore shape necessary to accommodate the NP (*SI Appendix*, Figs. S3 and S4). The portion of the NP that is physically "trapped" within the pore when it interacts with the substrate is defined as the "trapped region." The optimal pore depth and corresponding pore shape are determined via three-dimensional (3D) modeling using the following rules: 1) the shape of the pore should at least encompass the top-down projection area of the trapped region (Fig. 2 *A–D*); 2) the pore shape should allow the NP to interact with the surface in one unique orientation.

For octahedral NPs, the design principle is relatively straightforward since such particles have only one type of facet (triangle) that can interact with the substrate. Therefore, by patterning triangular shallow pores, the orientation of octahedra can be precisely controlled (Fig. 2*A*). For NPs with more than one type of facet shape, such as cuboctrahedra (with square and triangular facets), facet-selective assembly can be achieved in a stepwise fashion using pores of different sizes/shapes (Fig. 2*D*). For example, due to the difference in area (and therefore, DNA coverage) between two anchoring facets, the two types of facets have different desorption

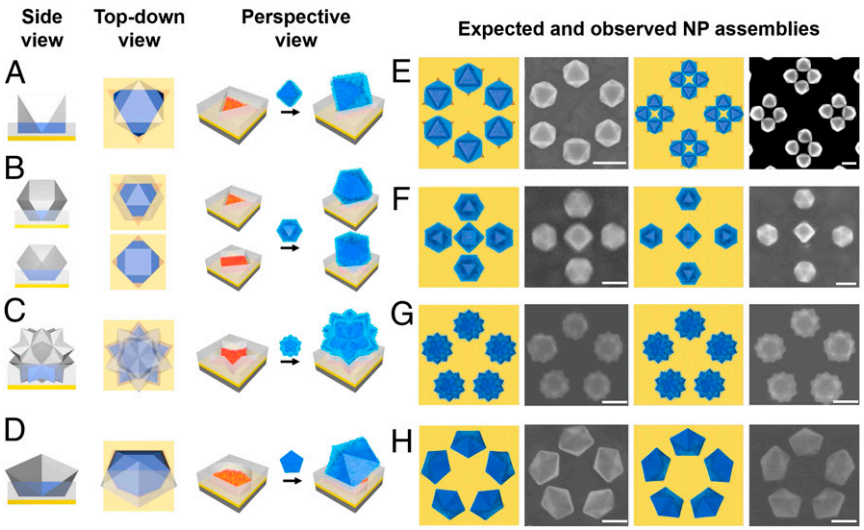

Fig. 2. Assembly of surface-bound NP architectures through facet-directed anchoring of anisotropic NPs (*A* and *E*) octahedral; (*B* and *F*) cuboctahedral; (*C* and *G*) small triambic icosahedron; and (*D* and *H*) decahedral. (*A–D*) show the lateral (side) and top-down views of single NPs when they are "trapped" into pores of ideal shapes and depth. The "trapped region," which is the portion of a NP that interacts with the pore, is highlighted in blue. In addition, for clarity, perspective views of the ideal pores and NP orientation achieved by embedding the NPs in these pores are shown. The region marked with red denotes the DNA that is attached to the gold substrate (yellow) at the bottom of the pore and is complementary to the DNA on the NPs. Note that for a cuboctahedron, two different facets can be selectively adsorbed onto the substrate by controlling the pore shape. Namely, when triangular pores (*B*, *Top*) are used, triangular facets interact with the substrate; while when square pores (*B*, *Bottom*) are used, the square facets can interact with the substrate. (*E–H*) present the schemes showing the top down view of an array of anisotropic NPs assembled at different orientations (colored images) and corresponding SEM images (grayscale images). [Scale bars: 100 nm (*E*, *F*, and *G*), 50 nm (*H*).]

temperatures (due to different amounts of DNA hybridization)—anchoring on the square facet yields an assembly with a higher melting temperature than when the assembly is anchored on the triangular facet. A slow cooling approach was taken to assemble each particle in a facet-directed manner into their corresponding pores—square facet-directed particle assembly was first realized with square pores at elevated temperature (~45 °C); triangular facet-directed particle assembly was then carried out with the triangular pores at room temperature (all of the larger square pores were filled). For more complex shapes, the pore design is more involved. For example, the top-down projection area of the trapped region of a small triambic icosahedron when the NP is resting on the surface is a five-sided star (Fig. 2*C*), while it is a heptagon (Fig. 2*D*) for a decahedron. These pore shapes can be determined in a straightforward manner via 3D modeling following the strategy delineated above.

We note that due to lithographic limitations, only pores with prismatic shapes can be fabricated by EBL. Therefore, it is nearly impossible to control the orientation of nonprismatic NPs, such as the ones used in this study, using deep pores. The shallow-template strategy, on the other hand, enables partial trapping of the NPs, which results in previously unobtainable control over particle position and orientation. Importantly, this strategy provides the opportunity to arbitrarily construct surface-bound architectures using NPs as building blocks with sub-10-nm precision in the x, y, and z directions. In addition, the oligonucleotide bonds between the NPs and the substrate can be reversibly expanded and contracted, providing dynamic control over the position of the NPs along the z direction.

The shallow-template strategy represents a significant advance over previous approaches toward building device-quality functional metamaterials with unprecedented surface morphologies. In addition, the oligonucleotide bonds between the NPs and substrate can be reversibly expanded and contracted, enabling postsynthetic tunabilities (15). Therefore, in principle, by controlling the interparticle distances between plasmonic NPs as well as their distance from the substrate, metamaterials that interact with and guide light in novel and unique ways may be realized. Indeed, guiding the propagation of light with NP-based structures has been a major theme in the field of optics. For example, controlled anomalous reflection using metasurfaces has been a target of interest since it can be used to design compact optical and photonic devices (30, 31). However, due to the limitations of traditional fabrication methods, creating metasurfaces with reconfigurable structures where each structural element corresponds to a specific functionality has remained a challenge. Here, we show that the shallow-template assisted, DNA-mediated assembly strategy allows one to address this challenge by providing access to in situ tunable metasurfaces that actively guide visible light along different directions in the reflection mode.

We designed a proof-of-concept, two-state metasurface based on finite-difference time-domain (FDTD) simulations. The metasurface was composed of 12 cubes arranged in a triangular formation, repeated across the entire substrate (Fig. 3*A* and *SI Appendix*, Fig. S7). The size of the cubes was chosen to be 80 nm, in part due to their optical activity and ease of synthesis. The periods (center of triangle to center of neighboring triangles) in the x and y directions were 320 and 750 nm, respectively. The distance between the individual cubes in both directions was 30 nm (Fig. 3 *A*, *Left Inset*). Such an arrangement of NPs leads to a metasurface that forms a spatial phase gradient that can reflect light in an anomalous direction (*SI Appendix*, Fig. S8). The metasurface exhibits high uniformity over a 700-μm × 700-μm area with a high yield of particles in the correct positions, as designed (Fig. 3*A*).

Through FDTD simulations, we first calculated the electromagnetic response of the overall structure to normal incident white light. The far-field optical power at collection angles between −90° and 90° was determined for two different distances between the NPs and the underlying gold substrate (3 and 20 nm). At a distance of 20 nm (expected length of the DNA in buffer solution), most of the power is reflected at 0°, as expected with conventional reflection (Fig. 3*B*). However, at a distance of 3 nm (expected length of the DNA in 80% EtOH solution), anomalous reflection near 60° was predicted over a relatively broad bandwidth from 610 to 690 nm. Specifically, the 670-nm wavelength was reflected to an anomalous angle of ~62° (*SI Appendix*, Fig. S9). The calculated electric-field distribution around the structure at 670 nm was consistent with this result (*SI Appendix*, Fig. S10). Our simulations suggest that the light intensity changes continuously at normal and anomalous angles as the DNA length decreases from 20 to 3 nm, yet the difference between the two extreme cases is enough to serve as an on/off optical switch.

We next proceeded to determine if the predicted optical behavior can be realized experimentally. However, from an experimental standpoint, it is challenging to detect the reflected power along the direction of the incident light. Based on the law of reciprocity, we reasoned that if incident 670-nm wavelength light was set at the angle of anomalous reflection (62°), the normal power would be guided to the other side with the same angle of reflection (the law of reflection), while the anomalous power would be guided to ~0°. We confirmed these expectations through another set of FDTD simulations (broadband simulation results, *SI Appendix*, Fig. S11). We then built an angle-resolved measurement setup that allows collimated light to illuminate a sample and measured the power of the reflected light at different collection angles using a rotational arm (*SI Appendix*, Figs. S12 and S13). The incident wavelength (670 nm) was chosen from the broadband light source with a bandpass filter. After passing through the focus and collimation lenses, the incident light was polarized perpendicularly to the y direction of the structure. The sample was placed in the imaging chamber (*SI Appendix*, Fig. S14) so that the distance between the NPs and the substrate could be dynamically modulated by controlling the DNA bond length using various concentrations of EtOH (32). We measured the reflected power around the anomalous (~0°) and normal (62°) angles of reflection for samples submerged in both buffer solutions containing 0% (20-nm DNA length) and 80% (3-nm DNA length) EtOH. As predicted, changing the EtOH concentration dramatically switched the metamaterial from a mirrorlike reflector to an anomalous reflector (broadband experimental results, *SI Appendix*, Fig. S15). Note that in addition to DNA exhibiting highly reversible contraction and expansion (32), the switch between two different device functions occurs within a fraction of a second, with no significant loss in performance after 10 cycles.

To conclude, we have developed a shallow-pore template strategy that when combined with DNA-mediated assembly allows the arrangement of NPs of any arbitrary shape onto a surface with nanometer precision. This versatile technique can be used to generate complex and highly tailorable systems with precise control over particle position, shape, and composition, in the form of optically active metamaterials. We have demonstrated an example of a two-state optical metasurface that can be structurally tuned to perform two distinct functions (normal or anomalous reflection). Importantly, this advance opens up the possibility of making structurally precise, dynamically responsive metamaterials on demand that can potentially lead to the development of difficult-to-fabricate structures with important functions, such as flat lenses, optical cloaking devices, and holograms. Moreover, fundamental studies based on this approach will likely provide insight into structure–function relationships, elucidating the role of structural parameters on optical performance and enabling the fabrication of large-scale devices based on hierarchical optical metamaterials.

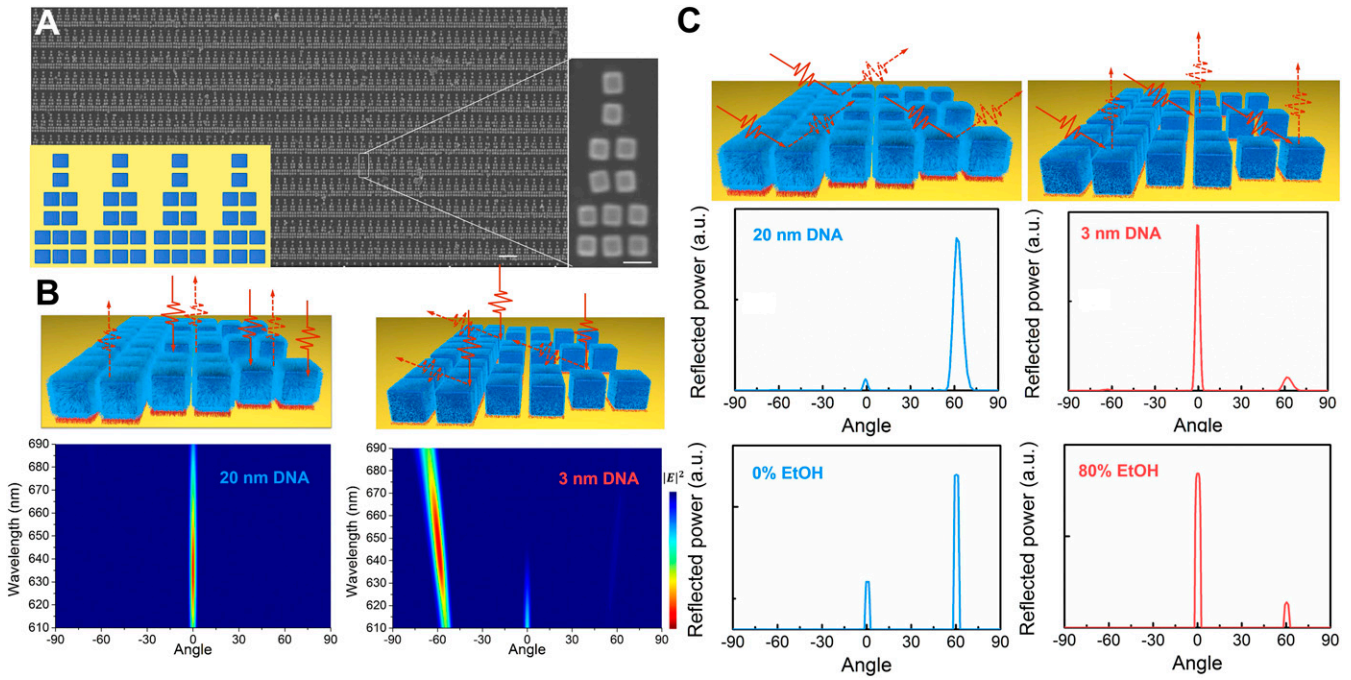

Fig. 3. Synthesis and characterization of a reconfigurable metasurface as an anomalous reflector. (*A*) Top-down scheme and SEM images of the synthesized metasurface, where a periodic array of 12 nanocubes are arranged on a gold substrate over 700 μm × 700 μm. (Scale bars: 1 μm; *Inset*: 100 nm.) (*B*) FDTD simulations of wavelength as a function of the reflected angle from the metasurface, where the gaps between nanocubes and the gold substrate are 20 nm (*Left*) and 3 nm (*Right*). (*C*) Simulated (*Top*) and experimental (*Bottom*) reflected power at 670 nm as a function of the reflected angle, where gaps between nanocubes and the gold substrate are 20 nm (0% EtOH) and 3 nm (80% EtOH), respectively.

Materials and Methods

Synthesis and Functionalization of Nanocrystals. All nanocrystals used in this work were synthesized through seed-mediated methods. Cubes, octahedra, and cuboctahedra were synthesized using single-crystalline seeds; decahedra were synthesized using pentatwinned seeds; small triambic icosahedra were synthesized using icosahedral seeds. As-synthesized nanocrystals were centrifuged and washed with H_2O to remove excess surfactant. Purified thiolated DNA was added directly to the nanocrystal solution. After the addition of thiolated DNA, the NP solutions were brought to 0.01 M sodium phosphate buffer (pH = 7.4) and 0.01 wt. % sodium dodecyl sulfate (SDS) in water. Stepwise addition of 2 M NaCl (aq) was then carried out every half hour, such that the NaCl concentration was stepped through 0.05, 0.1, 0.2, 0.3, 0.4, and 0.5 M after each successive addition. Following the last NaCl addition, the nanoparticles were placed on a shaker at 1,000 rpm and left overnight to ensure a dense loading of oligonucleotides.

Fabrication of Surface Template. Polymer templates were fabricated on Au-coated Si substrates using EBL. A p-doped <100> Si wafer with 500-μm thickness from NOVA Electronic Materials was cleaned via an O_2 plasma at 50 W for 30 min. Following plasma cleaning, electron beam evaporation (Kurt J. Lesker Company) was used to deposit a 5-nm Cr adhesion layer, followed by a 100-nm Au layer onto the Si substrate. Directly prior to NP assembly, Au substrates were spin-coated with positive e-beam resist (496 PMMA A2, MicroChem) at 4,000 rpm in order to achieve a 50-nm-thick layer of PMMA. We note that other PMMA thicknesses can be achieved by changing the spin speed as well as the PMMA concentration and solvent type (*SI Appendix*, Table S2) (28). The PMMA was prebaked at 200 °C for 60 s and then an FEI Quanta scanning electron microscope (SEM) was used to fabricate patterns of pores into the PMMA via EBL. Specifically, we used an accelerating voltage of 30 kV with a dosage of 120–200 $\mu C/cm^2$, depending on the desired pattern arrangement and PMMA thickness. The substrates were then developed in a methyl isobutyl ketone/isopropyl alcohol (IPA) 1:3 solution for 60 s, rinsed with IPA, and blown dry with N_2. The substrates were then cleaned with O_2 plasma at 50 W for 60 s to remove any residual PMMA on the Au surface at the base of each pore. It is important to note that, in principle, nearly any symmetry or spacing between NPs could be achieved simply by making a desired 2D arrangement of pores. After development, the substrates were cut into four smaller pieces, each roughly 7.5 mm by 7.5 mm, which allowed them to fit in the bottom of 2-mL Eppendorf tubes.

Assembly of Nanocrystals. DNA-functionalized nanocrystals are allowed to assemble onto specific binding sites of substrates with complementary DNA under shaking at 1,000 rpm at specific temperatures. The assembly process is typically finished in less than 2 h. For cuboctahedral nanocrystals, a decrease in temperature is required for two types of facets to register correctly. Therefore, the substrate–-NP solution mixture was shaken in 1-h increments at temperatures of 50, 45, 40, 35, 30, and 25 °C. The substrates after assembly were rinsed with 0.5 M NaCl buffer solution three times to wash off NPs that are not connected to the substrate by DNA-specific interactions. After NP assembly, the PMMA template was removed, and the substrates were dried prior to characterization using SEM. Specifically, the substrates were rinsed three times with a solution containing 80% IPA, 0.2 M ammonium acetate (AA), and 0.01% SDS. After the last rinse, the substrates were left in 80% IPA, 0.2 M AA, and 0.01% SDS at 45 °C for 30 min to fully remove the PMMA. Note that in addition to removing the PMMA, the alcohol reduces the solvent polarity around the DNA-assembled nanoparticle architectures, which condenses the DNA bonds between NPs and allows structures to be transferred intact from the solution phase to the solid state (*SI Appendix*, Fig. S4). After PMMA removal, the substrates were rinsed three times with a solution of 80% IPA and 0.2 M AA, then blown dry with N_2.

Data Availability. All study data are included in the article and *SI Appendix*.

ACKNOWLEDGMENTS. We thank V. P. Dravid (Northwestern University) for helpful discussions. This material is based on work supported by the following grants: Air Force Office of Scientific Research Award FA9550-17-1-0348 (Nanoparticle synthesis and assembly, Optical simulations and characterizations); Center for Bio-Inspired Energy Science, an Energy Frontier Research Center funded by the US Department of Energy, Office of Science, Basic Energy Sciences Award DE-SC0000989 (Oligonucleotide synthesis); and the Vannevar Bush Faculty Fellowship Program sponsored by the Basic Research Office of the Assistant Secretary of Defense for Research and Engineering and funded by the Office of Naval Research through Award N00014-15-1-0043 (EM characterization). Z.H. acknowledges support by the Northwestern University Graduate School Cluster in Biotechnology, Systems, and Synthetic Biology, which is affiliated with the Biotechnology Training Program funded by National Institute of General Medical Sciences Grant T32 GM008449. K.A. acknowledges support by the Office of Naval Research Young Investigator Program Award

(N00014-17-1-2425). This work made use of the Electron Probe Instrumentation Center of the Northwestern University Atomic and Nanoscale Characterization Experimental Center, which has received support from the Soft and Hybrid Nanotechnology Experimental Resource (NSF cooperative agreement award NNCI-1542205); the International Institute for Nanotechnology (IIN); the Keck Foundation; and the State of Illinois, through the IIN.

1. A. Alù, Metamaterials: Prime time. *Nat. Mater.* **15**, 1229–1231 (2016).
2. B. Luk'yanchuk *et al*., The Fano resonance in plasmonic nanostructures and metamaterials. *Nat. Mater.* **9**, 707–715 (2010).
3. Z. G. Nicolaou, A. E. Motter, Mechanical metamaterials with negative compressibility transitions. *Nat. Mater.* **11**, 608–613 (2012).
4. A. V. Kildishev, A. Boltasseva, V. M. Shalaev, Planar photonics with metasurfaces. *Science* **339**, 1232009 (2013).
5. M. Khorasaninejad *et al*., Metalenses at visible wavelengths: Diffraction-limited focusing and subwavelength resolution imaging. *Science* **352**, 1190–1194 (2016).
6. A. I. Kuznetsov, A. E. Miroshnichenko, M. L. Brongersma, Y. S. Kivshar, B. Luk'yanchuk, Optically resonant dielectric nanostructures. *Science* **354**, aag2472 (2016).
7. E. Arbabi *et al*., MEMS-tunable dielectric metasurface lens. *Nat. Commun.* **9**, 812 (2018).
8. K. H. Matlack, M. Serra-Garcia, A. Palermo, S. D. Huber, C. Daraio, Designing perturbative metamaterials from discrete models. *Nat. Mater.* **17**, 323–328 (2018).
9. M. Jang *et al*., Wavefront shaping with disorder-engineered metasurfaces. *Nat. Photonics* **12**, 84–90 (2018).
10. J. Valentine *et al*., Three-dimensional optical metamaterial with a negative refractive index. *Nature* **455**, 376–379 (2008).
11. M. Grzelczak, J. Pérez-Juste, P. Mulvaney, L. M. Liz-Marzán, Shape control in gold nanoparticle synthesis. *Chem. Soc. Rev.* **37**, 1783–1791 (2008).
12. V. Flauraud *et al*., Nanoscale topographical control of capillary assembly of nanoparticles. *Nat. Nanotechnol.* **12**, 73–80 (2017).
13. Y. Zhou *et al*., Shape-selective deposition and assembly of anisotropic nanoparticles. *Nano Lett.* **14**, 2157–2161 (2014).
14. Q.-Y. Lin *et al*., DNA-mediated size-selective nanoparticle assembly for multiplexed surface encoding. *Nano Lett.* **18**, 2645–2649 (2018).
15. Q.-Y. Lin *et al*., Building superlattices from individual nanoparticles via template-confined DNA-mediated assembly. *Science* **359**, 669–672 (2018).
16. L. Lin, M. Chen, H. Qin, X. Peng, Ag nanocrystals with nearly ideal optical quality: Synthesis, growth mechanism, and characterizations. *J. Am. Chem. Soc.* **140**, 17734–17742 (2018).
17. T. Das Gupta *et al*., Self-assembly of nanostructured glass metasurfaces via templated fluid instabilities. *Nat. Nanotechnol.* **14**, 320–327 (2019).
18. C. A. Mirkin, R. L. Letsinger, R. C. Mucic, J. J. Storhoff, A DNA-based method for rationally assembling nanoparticles into macroscopic materials. *Nature* **382**, 607–609 (1996).
19. S. Y. Park *et al*., DNA-programmable nanoparticle crystallization. *Nature* **451**, 553–556 (2008).
20. R. J. Macfarlane *et al*., Nanoparticle superlattice engineering with DNA. *Science* **334**, 204–208 (2011).
21. J. I. Cutler, E. Auyeung, C. A. Mirkin, Spherical nucleic acids. *J. Am. Chem. Soc.* **134**, 1376–1391 (2012).
22. R. J. Macfarlane, M. R. Jones, B. Lee, E. Auyeung, C. A. Mirkin, Topotactic interconversion of nanoparticle superlattices. *Science* **341**, 1222–1225 (2013).
23. M. R. Jones, N. C. Seeman, C. A. Mirkin, Nanomaterials. Programmable materials and the nature of the DNA bond. *Science* **347**, 1260901 (2015).
24. Y. Kim, R. J. Macfarlane, M. R. Jones, C. A. Mirkin, Transmutable nanoparticles with reconfigurable surface ligands. *Science* **351**, 579–582 (2016).
25. C. R. Laramy *et al*., Controlled symmetry breaking in colloidal crystal engineering with DNA. *ACS Nano* **13**, 1412–1420 (2019).
26. W. Zhou, Q. Y. Lin, J. A. Mason, V. P. Dravid, C. A. Mirkin, Design rules for template-confined DNA-mediated nanoparticle assembly. *Small* **14**, 1802742 (2018).
27. Q. Y. Lin *et al*., Strong coupling between plasmonic gap modes and photonic lattice modes in DNA-assembled gold nanocube arrays. *Nano Lett.* **15**, 4699–4703 (2015).
28. MicroChem, Nano PMMA and copolymer. https://kayakuam.com/wp-content/uploads/2019/09/PMMA_Data_Sheet.pdf. Accessed 12 November 2019.
29. X. Chen *et al*., Plasmonic focusing in rod-sheath heteronanostructures. *ACS Nano* **3**, 87–92 (2009).
30. Z. Li, E. Palacios, S. Butun, K. Aydin, Visible-frequency metasurfaces for broadband anomalous reflection and high-efficiency spectrum splitting. *Nano Lett.* **15**, 1615–1621 (2015).
31. S. Sun *et al*., High-efficiency broadband anomalous reflection by gradient metasurfaces. *Nano Lett.* **12**, 6223–6229 (2012).
32. J. A. Mason *et al*., Contraction and expansion of stimuli-responsive DNA bonds in flexible colloidal crystals. *J. Am. Chem. Soc.* **138**, 8722–8725 (2016).